Chemical, Electronic, and Electrical Properties of Alkylated Ge(111) Surfaces

ARTICLE *in* THE JOURNAL OF PHYSICAL CHEMISTRY C · JULY 2010

Impact Factor: 4.77 · DOI: 10.1021/jp101375x · Source: OAI

Chemical, Electronic, and Electrical Properties of Alkylated Ge(111) Surfaces

David Knapp, Bruce S. Brunschwig, and Nathan S. Lewis*

Beckman Institute and Kavli Nanosciences Institute, Division of Chemistry and Chemical Engineering, 210 Noyes Laboratory, 127-72, California Institute of Technology, Pasadena, California 91125

Received: February 13, 2010; Revised Manuscript Received: May 3, 2010

The use of Ge in semiconductor electronics has been constrained by the lack of a simple method of passivating the crystal surface. Toward that end, we have explored the utility of chemically bonded hydrocarbon monolayers. Alkylated Ge(111) surfaces have been prepared by addition of 1-alkenes to the H-terminated Ge(111) surface as well as by a two-step halogenation/alkylation procedure. The chemical compositions of the resulting methyl-, ethyl-, and decyl-terminated surfaces have been evaluated using X-ray photoelectron spectroscopy (XPS). Thermal addition of 1-decene produced hydrophobic surfaces with 0.3 ± 0.1 monolayer of Ge oxide detected by XPS, whereas no oxide was observed on the methyl-, ethyl-, or decyl-terminated surfaces that were prepared using the two-step halogenation/alkylation method. Methyl-terminated Ge(111) surfaces prepared by the two-step method displayed a well-resolved C 1s XPS peak at a binding energy of 284 eV, consistent with carbon bonded to a less electronegative element such as Ge. The electronic properties of all of the alkylated surfaces were characterized by measurements of the surface recombination velocity as a function of an externally applied gate voltage. Treatment of HF-etched Ge(111) surfaces with Br_2 vapor, followed by reaction with alkylmagnesium or alkyllithium reagents, yielded air-stable surfaces that had surface recombination velocities of 100 cm s^{-1} or less under flat-band conditions. The field-dependent surface recombination velocity experiments indicated that, in contact with air, methyl-terminated n-type Ge(111) samples had a negative surface potential approaching 300 mV, in contrast to the oxidized Ge(111) surface, which exhibited a strongly positive surface potential under the same conditions. Mercury contacts to n-type methyl-, ethyl-, or decyl-terminated Ge(111) substrates that were alkylated using the two-step method formed rectifying junctions with barrier heights of 0.6 ± 0.1 eV, whereas no measurable rectification was observed for Hg contacts to p-type Ge(111) substrates that were alkylated by the two-step method, to n-type Ge(111) substrates that were alkylated through addition of 1-decene, or to oxidized n-type Ge(111) samples.

I. Introduction

Si and Ge have a long history in the field of semiconductor electronics, but Si became dominant because the ability to form a stable, low defect density Si/SiO_2 interface allowed the development of the field-effect transistor. As device scaling to ever smaller feature sizes requires that the SiO_2 layer be replaced with high-κ dielectrics, that advantage is not as important. Because the hole carrier mobility in Ge is 4 times that in silicon, Ge provides an advantage in high-speed circuits and is of interest in CMOS technology, where the p-channel component of Si has traditionally had less than ideal performance.[1,2] Further, the 0.67 eV band gap of Ge allows the absorption of infrared radiation, which makes Ge, or a SiGe alloy, a suitable rear absorber in a multijunction solar cell.[3,4] Hence, methods that yield low defect-density Ge surfaces are of interest. For such techniques to be applicable to SiGe alloys or to Ge structures that are grown on a Si wafer, all of the processes must be compatible with Si.

The high surface-state density, and the instability and water solubility of Ge oxide, have proven to be significant drawbacks to the development of Ge-based technology.[5,6] A recent method of reducing the high surface-state density in Ge devices involves deposition of a layer of Si, to facilitate the growth of a conventional, low-defect Si suboxide, followed by growth of a high-κ material on the Si oxide.[7] Such techniques require the formation of overlayers of greater than 0.5 nm thickness and thereby necessarily introduce additional underside capacitance to the device, so direct chemical modification of the Ge crystal surface is of significant interest.[2]

Alkylation of Ge surfaces, by replacing the oxide of Ge(111) with a layer of grafted ethyl groups, has been shown to eliminate the sensitivity of the electrical properties to ambient moisture. However, such ethylated-Ge surface possess a high density of surface states.[8] The etching and halogenation steps used in these ethylation methods were harsh and may have caused appreciable roughening of the Ge surface. Possibly because of the high surface-state density, as well as the development of the thermal oxide on Si, little work has subsequently been performed with such Ge surfaces. In contrast to hydrogen termination of Si, which yields a metastable surface that is useful in processing, hydrogen-terminated Ge surfaces are not stable.[9,10] Sulfide passivation eliminates Ge oxides but can lead to the formation of a GeS glass.[1,11–15] Alkanethiols allow for the attachment of organic groups to the Ge surface through a Ge−S bond, but long-term stability has not been demonstrated.[10,16–18] In a method very similar to what has been used on silicon, 1-alkenes can be grafted to the H−Ge(111) surface to form a stable C−Ge bond.[17,19–22]

Improvements to the halogenation/alkylation technique have been developed for Si and have been shown to produce alkylated Si surfaces of high surface perfection that exhibit accordingly low densities of electronic defects.[23–26] Functionalization of H−Si(111) by the thermal addition of 1-alkene groups opens

* To whom correspondence should be addressed. E-mail: nslewis@caltech.edu.

10.1021/jp101375x
Published on Web 06/28/2010

the possibility of attachment of a wider variety of useful chemical species; however, the process yields surfaces of varying degrees of interface quality.[27–33] The work described herein has thus explored in depth the two-step halogenation/alkylation method as an approach to the production of stable Ge(111) surfaces with a low density of recombination centers. The chemical compositions of the resulting functionalized Ge surfaces have been characterized using X-ray photoelectron spectroscopy (XPS), the electronic properties have been characterized by measurements of the surface recombination velocity as a function of an externally applied gate voltage, and the electrical junction behavior of such surfaces has been determined by formation of Hg contacts and subsequent characterization of their device properties using differential capacitance and current−voltage measurements.

II. Experimental Section

A. Materials. Unless otherwise stated, chemicals were obtained from Aldrich or Alfa Aesar and were used as received. Water was obtained from a Barnstead NanoPure system and had a resistivity of 18 MΩ cm. 10 M HF(aq) solutions were made from by the dilution of 30 M (48 wt %) HF (Transene). Diethylene glycol dibutyl ether (DEGDBE) was vacuum-distilled from $LiAlH_4$ and was stored under N_2(g) until use. 1-Decene was vacuum-distilled from Na metal and stored in the dark, under N_2(g), until further use. Br_2(l) was vacuum-transferred from P_2O_5, then subjected to several freeze−pump−thaw cycles, and stored in a Schlenk flask until use.

Low vapor pressure organomagnesium or organolithium solutions were prepared from the corresponding diethyl ether solutions by addition of an equal volume of DEGDBE, followed by vacuum removal of the diethyl ether into a N_2(l) trap. Dimethylmagnesium was prepared by addition of small amounts of 1,4-dioxane to methylmagnesium bromide in diethyl ether until the $MgBr_2$·dioxane complex ceased to precipitate, after which the solution was passed through baked glass wool to remove the precipitate.[34] Two-inch diameter, 500 μm thick, Ge(111) wafers (MTI Corp.) were cut with a diamond scribe into sizes appropriate for the specific measurement and were sanded when necessary for ohmic contact formation. To remove contamination and Ge dust, the fragments were rinsed with water, dried with N_2(g), immersed in 10 M H_2O_2(aq) for 30−50 s, rinsed with water, and then dried.

B. Surface Modification. Immediately prior to surface modification, the Ge substrate was cleaned by suspending the sample for minimum of 45 min in a Soxhlet extractor that contained boiling isopropanol. The sample was then dipped in water, followed by etching in 10 M HF(aq) for 20 min, to form a hydrophobic surface. The surface was then blown dry with N_2(g) and immediately placed into a custom built drying chamber equipped with two Schlenk storage flasks that allowed for the addition of reagents without opening the chamber or exposing the chemicals to any materials other than glass and the fluorocarbon stopcock. The chamber was evacuated to <20 mTorr and backfilled several times with Ar(g). In the case of Si(111), the substrate was briefly etched with 30 M HF(aq), rinsed with water, and etched with degassed 11 M NH_4F(aq) (Transene) for 20 min prior to transfer of the sample into the drying chamber. Subsequent steps were identical to those used with the Ge samples.

For the halogenation/alkylation method, when the pressure had decreased to <20 mTorr, the drying chamber was isolated from the vacuum and backfilled with Br_2 vapor for 1−3 min. The vapor was then pumped off, and when the pressure had decreased to <20 mTorr, the low vapor pressure organomagnesium solution was added to the chamber until the sample was fully immersed in liquid. The chamber was kept under a positive pressure of Ar(g) and was heated to 60 °C for 3−12 h. After the chamber had cooled, the substrate was removed and rinsed with methanol. The sample was then briefly dipped in a 10% acetic acid solution to remove the magnesium alkoxides and was then rinsed sequentially with methanol, isopropanol, hexanes, isopropanol, and methanol. The same procedure was used to alkylate hydrogen-terminated Si(111).

For thermal hydrogermylation, an identical etching procedure was followed as for the two-step alkylation process. The drying chamber that contained a hydrogen-terminated Ge(111) sample was evacuated to <20 mTorr, and then 1-decene was added to the drying chamber, until the substrate was completely immersed in liquid. The chamber was kept under a positive pressure of Ar while the 1-decene was brought to reflux for 2 h. Once the chamber had cooled, the substrate was removed, and the Ge was rinsed with hexanes, followed by a rinse with isopropanol.

C. Instrumentation. X-ray photoelectron spectroscopy was performed at pressures of 10^{-9}−10^{-8} Torr on an M-Probe spectrometer that was interfaced to a computer running the ESCA2000 (Service Physics) software. The monochromatic X-ray source was the 1486.6 eV Al Kα line, directed at 35° to the sample surface. Emitted photoelectrons were collected by a hemispherical analyzer that was mounted at an angle of 35° with respect to the sample surface. The samples were conductive so charge neutralization was not needed. Low-resolution survey spectra were acquired between binding energies of 1−1100 eV. Higher-resolution detailed scans, with a resolution of ∼0.8 eV, were collected on individual XPS lines of interest. All binding energies are reported in electron-volts.

The conductance of the samples was monitored by passing a constant 0.5 mA current through a 10 mm by 20 mm rectangular, double-side polished substrate that had a Ga/In ohmic contact on each of the shorter edges of the samples. Photoconductivity decay (PCD) transients were initiated with a 20 ns pulse from a 1550 nm laser diode (Laser Components, Inc.) that was driven by an ETX-10A laser driver (Electro-Optic Devices). From the peak conductance, the injection intensity was determined to be $<10^{12}$ cm^{-3} for low-level injection conditions. The surface potential was varied by clamping the sample between two 10 mm wide glass field plates that had been coated with F-doped tin oxide, so that a 1 cm^2 gate region was formed on each side of the sample. The field plates were separated from the sample surface by hydrocarbon oil as well as by a 10−13 μm film of poly(vinyl fluoride) (Goodfellow), resulting in a capacitance of 300 pF cm^{-2}. The gate bias was supplied by two 2.5 W 1 kV JB series power supplies (Matsusada) and was controlled by a custom-built circuit. Qualitative conductance measurements performed under vacuum were conducted in a high-vacuum (10^{-7} Torr) load-lock attached to the XPS system, and the field plates were separated from the sample surface only by the fluoropolymer film.

Barrier-height measurements were conducted on 1 cm^2 single-side polished samples that were prepared as described above. Ohmic contacts were formed with Ga/In across the rough side of the sample, and the sample was then placed rough-side down on a copper bar. Hg/Ge junctions were formed by containing electronic-grade Hg within a fluorocarbon elastomer O-ring that was held against the polished side of the Ge sample. A platinum wire was touched to the Hg to form an electrical lead without forming an amalgam or altering the work function of the Hg. The junction was connected to a model 1287 Solartron poten-

tiostat operated in a two-electrode configuration, with the copper bar as the working electrode and the platinum wire as the counter electrode. Current−voltage ($I-V$) data were collected, using the Corrware software package (Scribner), at a scan rate of 10 mV s^{-1}, between −0.4 and 0.6 V. Impedance measurements were made with a Schlumberger SI 1260 frequency response analyzer that was controlled by the Zplot software package (Scribner). The ac voltage was 10 mV, and the swept frequency range was typically 10^1-10^6 Hz.

D. Data Analysis. The methods used to analyze the XPS data have been described previously.[35] The hydrocarbon overlayer thickness, d_{ov}, was computed by use of the relationship

$$d_{ov} = \lambda_{ov} \sin\theta \times \ln\left[1 + \left(\frac{SF_{Ge}}{SF_{ov}}\right)\left(\frac{I_{ov}}{I_{Ge}}\right)\left(\frac{\rho_{Ge}}{\rho_{ov}}\right)\right] \quad (1)$$

where I is the peak intensity, ρ is the atomic density, SF is the sensitivity factor, λ is the photoelectron escape length, and θ is the photoelectron takeoff angle determined by the surface orientation relative to the analyzer. The subscript "ov" signifies an overlayer component; the subscript "Ge" signifies a Ge component. The Ge 3d spectral peak was chosen rather than the more surface sensitive Ge 2p peak because the Ge 3d photoelectron has a kinetic energy close to that of the C1s photoelectron, so that $\lambda_{Ge} \approx \lambda_{ov}$. The coverage of oxide in fractional monolayers was calculated by comparing the measured $I_{Ge,s}/I_{Ge}$ ratio to the maximum computed from

$$\frac{I_{Ge,s}}{I_{Ge}} = \frac{n_{Ge,s}}{n_{Ge}\lambda_{Ge,bulk}\sin\theta - I_{Ge,s}} \quad (2)$$

where $I_{Ge,s}$ is the intensity of the higher binding energy component of the Ge 3d peak that is distinct from the bulk component. The bulk atomic density, n_{Ge}, and the surface atomic density, $I_{Ge,s}$ were assigned values of 4.42×10^{22} cm^{-3} and 7.4×10^{14} cm^{-2}, respectively.[37,38] The value used for a 100% oxidation ratio is 0.223.

The change in conductance, $\Delta\sigma$, relative to flat-band conditions was obtained from the measured resistance, R, by[37]

$$\Delta\sigma - \Delta\sigma_{min} = \frac{l}{2w}\left(\frac{1}{R} - \frac{1}{R_{max}}\right) \quad (3)$$

where l and w are the sample length and width, respectively; $\Delta\sigma_{min}$ and R_{max} are the conductance (relative to the flat-band value) and resistance, respectively, of the sample as the surface transitioned between inversion and depletion conditions. The surface potential was derived through the functional relationship depicted in Figure 1. These functional relationships were generated numerically with a computer script available in the Supporting Information.

Surface recombination velocities, S, were calculated from the measured single-exponential decay constant, τ, of the photoconductivity decay transient by[38]

$$S = \frac{d}{2}\left(\frac{1}{\tau} - \frac{1}{\tau_b}\right) \quad (4)$$

where τ_b is the bulk lifetime of 1.5 ms and d is the wafer thickness.

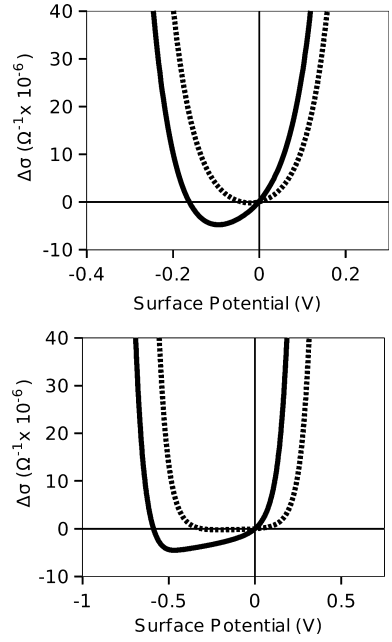

Figure 1. Functional relationships between surface conductance, $\Delta\sigma$, and surface potential, V_s, calculated for (a) intrinsic (dashed line) and lightly doped n-type (solid line) Ge and (b) high resistivity n-type (dashed line) and moderately doped n-type (solid line) Si.[37]

Barrier heights, Φ_{Bn}, were calculated from the saturation current of the current density vs voltage by

$$\Phi_{Bn} = \frac{kT}{q}\ln\left(\frac{A^{**}T^2}{J_{ST}}\right) \quad (5)$$

where J_{ST} is the saturation current density obtained by extrapolating the forward current density to zero bias, k is the Boltzmann constant, T is absolute temperature, A^{**} is the modified Richardson constant, taken as 50 A cm^{-2} K^{-2}, and q is the (unsigned) electronic charge.[36] Barrier heights were also determined through measurement of the differential capacitance of the depletion region, C_{sc}, by

$$\left(\frac{C_{sc}}{A}\right)^{-2} = \left(\frac{2\left(-V + V_{bi} + \frac{kT}{q}\right)}{q\varepsilon\varepsilon_0 N_D}\right) \quad (6)$$

where ε is the dielectric constant of Ge, ε_0 is the permittivity of free space, and N_D is the bulk dopant density. The built-in voltage, V_{bi}, is given by

$$V_{bi} = \Phi_{Bn} - \frac{1}{q}(\mathbf{E}_F - \mathbf{E}_i) \quad (7)$$

where $\mathbf{E}_i$ and $\mathbf{E}_F$ are the intrinsic Fermi level and the actual Fermi level, respectively.

III. Results

A. Surface Chemical Analysis. Figures 2 and 3 show representative XPS data obtained from alkyl-terminated surfaces. The survey spectra of methyl-terminated Ge(111) surface and of a sputter-cleaned bare Ge(111) surface (Figure 2a) indicated that little if any oxygen was detectable on the methylated Ge surface. The high-resolution C 1s spectrum of the methyl-

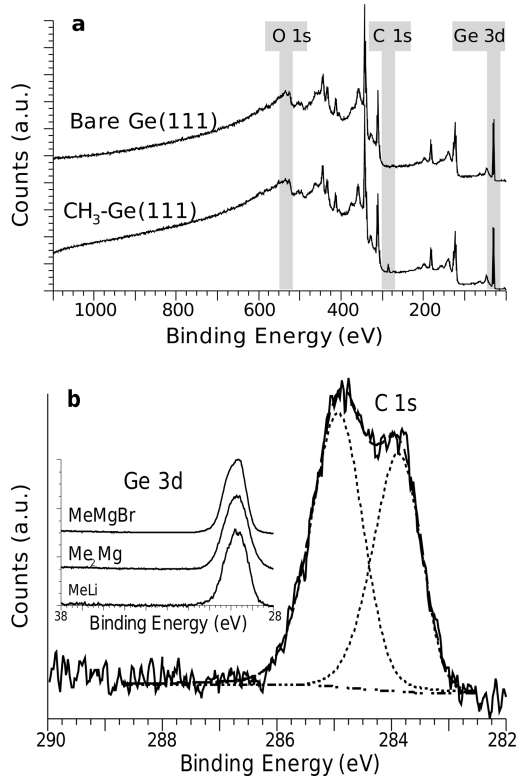

Figure 2. XPS of methyl-terminated Ge(111) surfaces. (a) A survey scan of a methyl-terminated Ge surface, compared with a bare Ge(111) surface prepared in UHV. The elemental peaks of interest are highlighted. (b) Detailed XPS scans of C 1s and Ge 3d (inset). The lower binding energy peak of the C 1s signal is assigned to the methyl carbon bonded to the Ge. The higher binding energy peak is assigned to adventitious hydrocarbon.

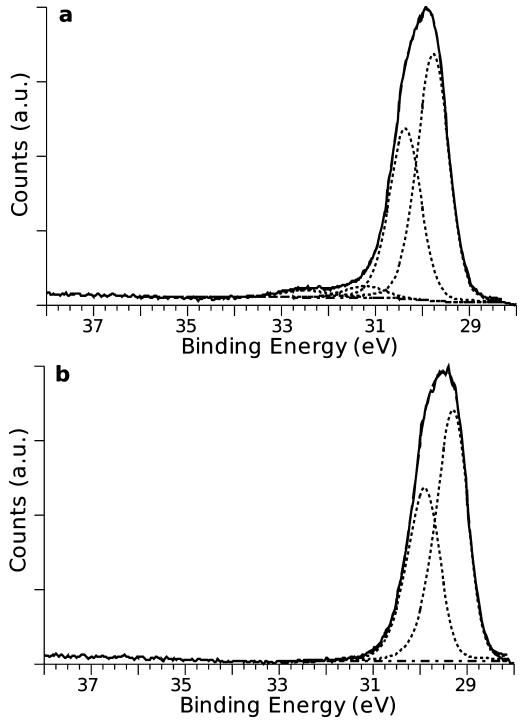

Figure 3. Detailed XPS scans of the Ge 3d peak of decyl-terminated Ge(111) surfaces prepared through (a) thermal hydrogermylation of 1-decene and (b) bromination/alkylation with decylmagensium bromide.

terminated Ge sample (Figure 2b) exhibited two clearly distinguishable peaks: one near 285 eV ascribable to C−C (due to adventitious hydrocarbon) and a second peak at 284 eV ascribable to the C−Ge of the surface-bound methyl group. For larger alkyl groups such as decyl, the peak at 285 eV became more intense and the peak at lower binding energy was not as clearly distinguishable in the XPS data (available in Supporting Information). The inset of the C 1s spectrum in Figure 2b shows the Ge 3d peak for samples that were prepared with three different methylating agents. Dimethylmagnesium, methyllithium, and methylmagnesium halide all reacted with the Br-terminated Ge(111) surface to produce a nearly oxide-free, methyl-terminated Ge(111) surface.

Figure 3a,b displays the Ge 3d peaks that were observed for decyl-terminated Ge(111) surfaces that were prepared through thermal hydrogermylation and through halogenation followed by Grignard alkylation, respectively. No oxide was detected on the Grignard-treated Ge(111) surface, but the surface that was treated with 1-decene reproducibly exhibited some level of oxidation above the detection limits of the instrumentation.

Table 1 presents the coverages of the various surface-bound species calculated from the XPS data. The peak area ratio of the lower binding energy component of the carbon peak to that of the bulk Ge 3d peak is in agreement with the ratio observed for the similar carbon component and bulk Si 2p peak areas that has been previously observed for methyl-terminated Si(111).[39]

B. Surface Conductance. For the undoped and n-type Ge(111) samples studied, a significant increase in sample conductance upon application of a negative bias to the sample with respect to the field plate, and a decrease in sample conductance upon application of a positive bias, indicated that the oxidized, etched, and 1-decene-treated Ge(111) surfaces were in accumulation in the absence of an applied field (i.e., the surface potential was on the right side of the curves in Figure 1). However, a quantitative determination of the surface potential could not be made for these samples because R_{max} of eq 3 was not accessible. The magnitude of the change in conductance in response to an applied field of a given strength decreased when any of these samples were under vacuum, relative to when they were exposed to air, indicating that the positive surface charge was produced by exposure to ambient conditions.

The field-dependent conductance data obtained for methyl-, ethyl-, and decyl-terminated Ge(111) surfaces prepared by the two-step halogenation/alkylation procedure indicated inversion conditions in the absence of an applied field (i.e., the sign of the response to an applied electric field indicated that the surface potential was on the left side of the curves in Figure 1). In addition, for such samples, R_{max} was attainable experimentally.

Figure 4 displays the surface recombination velocity data as a function of the applied field voltage for various Ge(111) surfaces that were prepared by the two-step halogenation/alkylation method. Most samples showed minimal surface recombination in the absence of an electric field applied normal to the surface, but samples with ethyl or decyl termination often displayed increased recombination as the surface was brought closer to flat-band conditions by application of a negative sample bias.

The maximum surface recombination velocity and the zero-applied-field surface potential of the measured samples for which R_{max} was reached (so the surface potential could be calculated from eq 3 and Figure 1) are reported in Table 2. The first index of the sample number indicates from which of three wafers the particular sample was cut (**1** and **3** being nominally undoped with a resistivity of 40−44 Ω cm, **2** being Sb doped with a resistivity of 15 Ω cm). In general, the samples with a more

TABLE 1: Hydrocarbon Coverage and Surface Oxidation As Determined by XPS

sample type	d_{ov}[a] (nm)	d_{ox} (nm)	I_C:I_{bulk}[b]	% oxidized
CH_3−Ge(111)	1.2 ± 0.2	−[c]	0.15 ± 0.02	−[c]
CH_3−Si(111)	1.3 ± 0.2	−[c]	0.13 ± 0.02	−[c]
1-decene + H−Ge	2.1 ± 0.2	0.20 ± 0.03	−[c]	30 ± 10
$C_{10}H_{21}MgBr$ + Br−Ge	2.2 ± 0.2	0.06 ± 0.06	−[c]	10 ± 10

[a] Overlayer thickness calculated from eq 1, using entire C 1s signal. [b] Ratio is normalized to the sensitivity factor of the substrate element with only the lower binding energy component of the C 1s considered. [c] No observable signal.

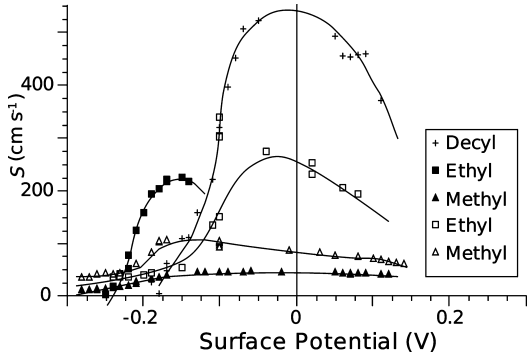

Figure 4. *S* as a function of surface potential for five Ge(111) samples modified with the two-step halogenation/alkylation process. Lines are for visual guidance only.

negative surface potential had a lower maximum surface recombination velocity. Such samples were mostly comprised of methyl-terminated Ge(111) samples that were prepared by the two-step halogenation/alkylation method.

Because alkylated surfaces prepared by the halogenation/alkylation method were under inversion at no applied field and because the external field was applied in a pulsed form, an estimate of the surface charge density could be obtained from the amplitude of the transient at the edge of the field pulse.[37] Figure 5a presents an example of the change in conductance that was observed when a negative square pulse sample bias was applied to a surface under inversion as a result of the two-step halogenation/alkylation procedure. Peak 1 is due to the onset of the applied field, and peak 2 is the laser-induced transient that was used to measure *S*. The change in conductance reflected in the amplitude of peak 1, $\Delta\sigma_1$, is proportional to the injected charge:

$$\Delta\sigma_1 = q(\mu_n + \mu_p)\Delta P \quad (8)$$

with the mobilities having their usual bulk values and where ΔP is the excess positive charge arising from the inversion layer. As the amplitude of the applied field was increased, and the resulting steady-state surface potential approached accumulation conditions, the amplitude of peak 1 reached a constant value, indicating that the entire inversion layer charge had been injected into the bulk. From these data, the charge in the inversion layer was calculated to be $(1-3) \times 10^{12}$ cm^{-2}.

For Si, analogous quantitative conductance vs field strength data could not be obtained with the instrumentation used because Si has a higher intrinsic resistivity, and a wider band gap, than Ge, which prevents the attainment of the conductance minimum for Si under most conditions. Nevertheless, the sign of the conductance response to an applied field provided some information for the alkylated Si(111) samples. Methyl termination of a lightly n-doped Si(111) substrate (the dashed curve of Figure 1b) produced surfaces that were in inversion at zero bias (qualitatively similar to the methyl-terminated Ge(111)), while a more heavily doped n-type substrate (solid curve) produced surfaces that were in depletion. These data thus indicate that such methyl-terminated Si(111) samples had a zero-field surface potential in the range of −200 to −400 mV.

C. Hg/Ge Junctions. As seen from the Mott−Schottky (C^2-V) and Nyquist plots displayed in Figure 6, Hg contacts to n-type Ge substrates modified through the halogenation/alkylation process formed Schottky contacts. At reverse bias, the depletion region capacitance dominated the impedance data, and the data were reasonably well-described by the conventional model circuit of a resistor in series with a parallel capacitor and resistor combination. The $\log(J)-V$ data were linear in forward bias, and the junctions had a diode quality factor of 1.3 ± 0.1. The barrier heights and diode quality factors deduced from a conventional thermionic emission analysis of such contacts for substrates of different dopant concentrations (denoted **I**−**V**) are presented in Table 3. At higher current densities, one would expect the thickness of the hydrocarbon in the overlayer to influence the $J-V$ data because under such conditions tunneling through the insulator will become the current-limiting process. However, at the low forward biases used in this work, the currents were governed by thermionic emission.[28,40] The junction capacitance dominated the impedance data for almost 2 decades at higher applied frequency, and the junction was well represented by the equivalent circuit depicted in Figure 6b (inset).

The oxide- and decyl-terminated n-type Ge(111) samples made by thermal addition of 1-decene, and all alkylated p-type Ge substrates, did not display measurable rectification in contact with Hg. Nominally undoped Ge(111) substrates (type **I** in Table 3) subjected to the two-step halogenation/alkylation process were rectifying, but all such samples displayed diode quality factors greater than 2, and their impedance data could not be well fit to the model circuit inset in Figure 6 to yield a parallel capacitance, regardless of the length of the alkyl chain.

IV. Discussion

A. Surface Chemical Analysis. The isopropanol reflux used to clean the substrate does not remove oxide, and the conditions of moist air and heat would be expected to lead to oxide growth on an unprotected Ge(111) surface. However, the lack of detectable oxygen on the methyl-terminated Ge(111) surfaces after exposure to refluxing isopropanol for as long as 12 h demonstrates the ability of the halogenation/alkylation method to produce stable, oxidation-resistant surfaces. The normalized I_{Ge}:I_{C-Ge} ratio for methyl-terminated Ge(111) surfaces was observed to be in accord with the I_{Si}:I_{C-Si} ratio observed for methyl-terminated Si(111) surfaces both in this work and in previously reported results.[39] Because methyl-terminated Si(111) has been shown to possess essentially complete local chemical passivation and because the lattice constant of Ge is similar to that of Si, the similarity between the XPS signal ratios of CH_3−Ge(111) and CH_3−Si(111) surfaces supports the notion that the two-step halogenation/methylation process completely functionalizes the Ge atop sites with methyl groups.[36]

TABLE 2: Surface Potential under No Applied Bias and the Maximum Surface Recombination Velocity within Available Bias Conditions for Functionalized Ge(111)

sample	$C_{10}H_{21}$ (**1**-0)	C_2H_5 (**1**-1)	C_2H_5 (**1**-2)	C_2H_5 (**1**-3)	CH_3 (**1**-4)	C_2H_5 (**2**-1)	C_2H_5 (**2**-2)	CH_3 (**2**-3)
$v_{s,0}$ (mV)	−140	−50	−140	−220	−270	−100	−100	−270
S_{max} (cm/s)	520	450	210	224	50	230	350	170
sample	C_2H_5 (**2**-4)	CH_3 (**2**-5)	C_2H_5 (**2**-6)	CH_3 (**3**-1)	C_2H_5 (**3**-2)	CH_3 (**3**-3)	C_2H_5 (**3**-4)	CH_3 (**3**-5)
$v_{s,0}$ (mV)	−100	−250	−210	−210	−140	−260	−170	−260
S_{max} (cm/s)	480	100	300	140	130	70	150	70

The spectrometer instrumentation used does not allow for the annealing process necessary to desorb the adventitious contaminants, so the contaminants complicate the measurement of the overlayer thickness for longer alkyl chains, such as the decyl groups, for which much of the alkyl group is spectroscopically indistinguishable from contaminants.[41] If the adventitious contamination layer can be assumed to be similar for both decyl- and methyl-terminated surfaces, a layer thickness of 1.4 ± 0.4 nm may be calculated by subtracting the total thickness calculated for the methyl overlayer observed by XPS (1.2 ± 0.2 nm) from the total XPS-derived thickness of the decyl-terminated layer (see Table 1). The value of 1.4 ± 0.4 nm for the overlayer thickness is within the range of reported thicknesses of decene monolayers, less 2 Å for the van der Waals diameter of the subtracted methyl carbon.[42,43]

To study the differences in oxide content between the decyl-terminated surface prepared using the two-step halogenation/alkylation reaction or thermal hydrogermylation, hydrofluoric acid was used to etch all samples studied so that differences in the resulting overlayers reflected differences in the reactions themselves, as opposed to differences in the methods of etching

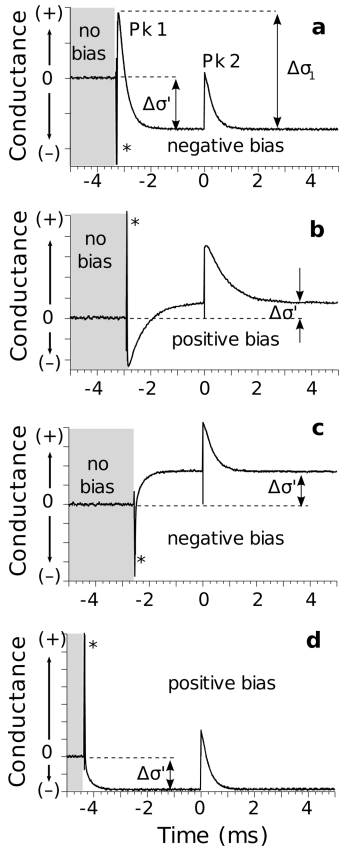

Figure 5. Conductance waveforms from which values for S and for the surface potential are derived. The peak at $t = 0$ is the rise in conductance due to pulsed-laser-generated carriers in the bulk crystal. Narrow peaks labeled with an asterisk are capacitive currents from the field plate at the onset of the bias. $\Delta\sigma'$ is the difference in conductance between when the sample was biased with respect to the field plate and when it was not biased. (a) A negative bias applied to a methyl-terminated Ge(111) surface. $\Delta\sigma_1$ is the change in conductance due to injection of charge associated with the inversion layer present before the application of the field. (b) Positive bias is applied to a methyl-terminated surface. (c, d) A negative bias and positive bias, respectively, is applied to an oxidized Ge(111) surface.

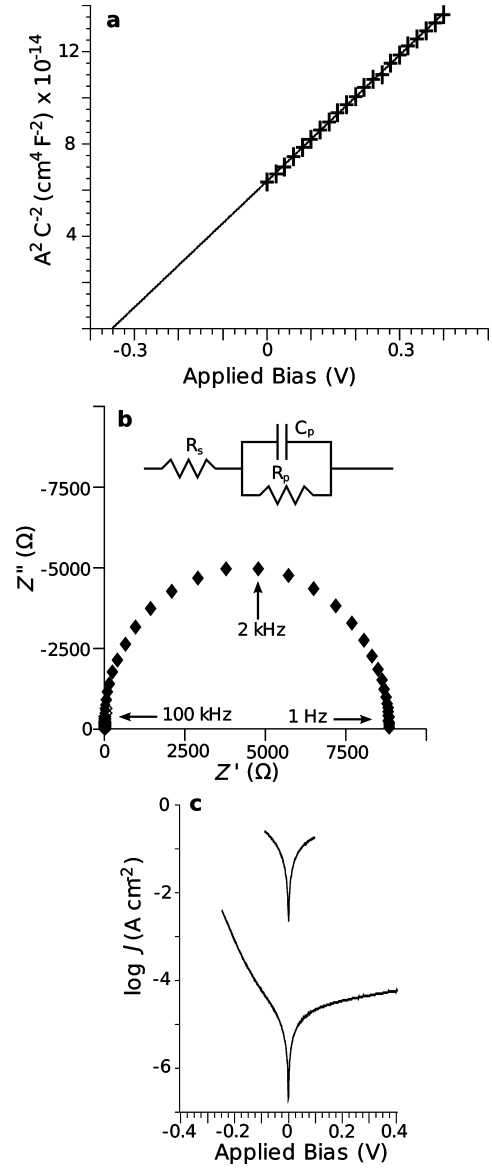

Figure 6. Representative electrical data for Hg contacted to a Grignard-derived decyl-terminated n-Ge(111) surface. (a) $C^{-2}-V$ plot. (b) Nyquist plot of the same junction at 200 mV reverse bias. (c) $J-V$ plot of the same sample (lower curve) and a decyl-terminated sample prepared via hydrogermylation (upper curve).

TABLE 3: Junction Properties of Hg Contacted to Functionalized Ge(111)

	$C^{-2}-V$ measurements		$J-V$ measurements	
sample type	N_D (cm^{-3})[a]	$\Phi_{Bn,C^{-2}-V}$ (V)	quality factor n	$\Phi_{Bn,J-V}$ (V)
CH_3-Ge **I**	N/A[b]	N/A[b]	2.0 ± 0.2	0.53 ± 0.05
$C_{10}H_{21}-Ge$ **I**	N/A[b]	N/A[b]	2.15 ± 0.08	0.52 ± 0.01
CH_3-Ge **II**	$(1.3 \pm 0.2) \times 10^{15}$	0.44 ± 0.12	1.6 ± 0.2	0.55 ± 0.05
C_2H_5-Ge **II**	$(3.6 \pm 0.4) \times 10^{14}$	0.67 ± 0.07	1.6 ± 0.2	0.55 ± 0.05
$C_{10}H_{21}-Ge$ **II**	$(3.7 \pm 0.4) \times 10^{14}$	0.56 ± 0.06	1.68 ± 0.2	0.57 ± 0.05
CH_3-Ge **III**	$(7.9 \pm 0.3) \times 10^{16}$	0.43 ± 0.03	1.45 ± 0.28	0.65 ± 0.03
C_2H_5-Ge **III**	$(7.9 \pm 1) \times 10^{16}$	0.61 ± 0.09	1.07 ± 0.02	0.67 ± 0.02
$C_{10}H_{21}-Ge$ **III**	$(4.6 \pm 0.4) \times 10^{16}$	0.63 ± 0.05	1.21 ± 0.04	0.61 ± 0.01
CH_3-Ge **IV**	$(6.7 \pm 0.6) \times 10^{15}$	0.52 ± 0.07	1.34 ± 0.11	0.60 ± 0.03
$C_{10}H_{21}-Ge$ **IV**	$(4.2 \pm 0.5) \times 10^{15}$	0.61 ± 0.04	1.15 ± 0.05	0.69 ± 0.01
CH_3-Ge **V**	$(1.1 \pm 0.4) \times 10^{17}$	0.47 ± 0.1	1.6 ± 0.2	0.65 ± 0.05
$C_{10}H_{21}-Ge$ **V**	$(0.9 \pm 0.4) \times 10^{17}$	0.8 ± 0.2	1.4 ± 0.3	0.63 ± 0.05

[a] Donor density as determined by the slope. [b] Not available; data could not be fit to equivalent circuit model in Figure 6b.

the surfaces.[44] Although the hydrogen-terminated Ge(111) surface is unstable in air, the low oxygen content of the surfaces prepared using the halogenation/alkylation process demonstrates that, with proper handling, Ge oxide growth can be minimized. Therefore, the oxide observed on the surfaces prepared by thermal hydrogermylation is most likely due to the instability of the hydrogen-terminated surface under reaction conditions such as the elevated reaction temperature.[16]

Unlike halogen-terminated Si(111) surfaces, halogen-terminated Ge(111) surfaces have been reported to be unreactive toward alkyllithium reagents.[45] A radical reaction pathway open to Grignard-treated Si should however also be available to alkyllithium reagents.[39,46,47] The XPS data reported here indicate that Br-terminated Ge(111) surfaces readily reacted with methyllithium to yield a surface that was nominally identical spectroscopically, electrically, and electronically to that obtained when the Br−Ge(111) surface was exposed to the methyl Grignard reagent.

B. Surface Conductance. The surface conductance results are in general accord with prior data on ethyl-terminated Ge surfaces.[48] However, for our system, a more complete conductance curve was obtained, and the point of maximum surface recombination was observable. This indicated that our system had either a lower surface state density or a higher field-plate capacitance. Prior work used an air gap between the semiconductor surface and the field plate, which allowed for the use of different gaseous atmospheres, but instability in such measurements has been reported to change the surface electronic properties.[5,6,48,49]

The surface potential of the oxidized Ge(111) surfaces was observed to be on the opposite side of the intrinsic Ge Fermi level from the surface potential of the Grignard-derived alkylated Ge(111) surfaces. The surface potential position of the alkylated samples that displayed less band bending, such as ethyl- or decyl-terminated Ge(111) surfaces, could be produced by the presence of surface oxides at levels below the detection threshold of the XPS instrumentation. This hypothesis is supported by the observation that such surfaces had generally higher values of S than the methyl-terminated Ge(111) surfaces that also displayed the strongest inversion at zero applied field.

The conductance results do not provide direct insight into the chemical nature of the charges on the alkylated Ge(111) surfaces. Nevertheless, the charge density and surface potentials observed for such surfaces are in general accord with behavior that has been proposed for dangling bonds.[51,52] The native oxide on Ge is of poor electronic quality and often yields a positive surface potential, likely due to the presence of moisture.[5] A dependence of the positive surface charge upon the presence of both oxide and water would explain the deduced shift in surface potential between vacuum and ambient conditions as well as the difference between the behavior observed for the oxidized surfaces and the observed threshold voltage shift seen in Ge p-MOS devices (the conduction is not off at zero gate bias).[52] The results of the two-step alkylation/halogenation can be explained if the alkyl termination, while not completely removing the acceptor states, prevents surface interaction of the Ge surface with water molecules.

Conductivity and scanning tunneling spectroscopy measurements indicate the presence of an inversion layer on Cl-terminated n-Si(111).[53,54] While alkylation of a halogen-terminated Ge(111) surface yields a surface that is predominately alkyl-terminated, a small number of halogen-terminated sites could be present in the system. The amount of charge in the inversion layer present in the methyl-terminated surface is consistent with 0.1−1% of the Ge(111) surface atoms remaining halogen-terminated. Such a concentration is well below the detection level of the XPS but is not insignificant. However, the lack of observation of persistent chlorine atoms in similarly prepared methyl-terminated Si(111) samples, for which there is also a shift in surface potential, makes it unlikely that unreacted halogen surface atoms are the cause of the surface charge.[41,43,55,56]

C. Hg/Ge Junctions. The poor rectification performance of Ge(111) surfaces that have XPS-detectable oxide is expected in light of the conductance data, which indicated n-type samples would be in accumulation. Although the XPS data show that the treatment of Ge(111) with 1-decene produces an alkyl overlayer, the method did not provide significant electrical passivation. Hg contacts to n-type Ge(100) samples treated with 1-octadecene have been reported to have a 0.41 eV barrier height, but such contacts had high ideality factors and positive surface charge, consistent with our observations.[20] The lack of rectification for Hg contacts to p-type substrates is consistent with the high barrier heights, approximately equal to the entire band gap, that were observed for n-type Ge(111) samples treated with the halogenation/alkylation procedure.

From the Ge conductance data reported herein and from previous data on Hg/Si(111) junctions, the methyl-terminated surfaces would be expected to exhibit a high barrier height due to a lack of oxide-related surface states and the shift in apparent electron affinity caused by the dipole of surface methyl groups.[57] The measured Hg/n-Ge barrier heights thus confirm the lack of pinning at a positive surface potential but do not distinguish

between ideal behavior or the pinning traditionally seen in solid-state Schottky contacts to n-Ge.

V. Conclusion

Alkylation of Ge(111) surfaces via the two-step halogenation/alkylation method provides air-stable, low oxygen content surfaces, with a low density of midgap recombination centers as evidenced by surface recombination velocities lower than 100 cm s^{-1} under depletion conditions. For undoped and lightly doped n-type substrates, such a passivation process causes a shift in surface potential approaching −300 mV. This behavior is in contrast to n-Ge(111) substrates with oxidized or etched surfaces or surfaces that had been alkylated by thermal hydrogermylation with 1-decene, which were in accumulation in contact with an air ambient. Hg contacts to n-Ge(111) substrates treated with the two-step halogenation/alkylation process exhibited barrier heights of 0.6 ± 0.1 V, and the differential capacitance vs voltage behavior of such junctions indicated near-ideal behavior, in contrast to substrates that were either left unprotected or modified with 1-decene, which showed little detectable rectification.

Acknowledgment. We acknowledge the National Science Foundation, Grant CHE-0604894, the Defense Advanced Research Projects Agency, Grant BAA-08-48, and the Beckman Institute for support of this work.

Supporting Information Available: C 1s XPS of decyl-terminated Ge(111) and the python script used to compute the surface conductance vs surface potential relationship in Figure 1. This material is available free of charge via the Internet at http://pubs.acs.org.

References and Notes

(1) Frank, M. M.; Koester, S. J.; Copel, M.; Ott, J. A.; Paruchuri, V. K.; Shang, H.; Loesing, R. *Appl. Phys. Lett.* **2006**, *89*, 112905.
(2) Brunco, D.; et al. *J. Electrochem. Soc.* **2008**, *155*, H552–H561.
(3) King, R.; Law, D.; Edmondson, K.; Fetzer, C.; Kinsey, G.; Yoon, H.; Sherif, R.; Karam, N. *Appl. Phys. Lett.* **2007**, *90*, 183516.
(4) Guter, W.; Schoene, J.; Philipps, S.; Steiner, M.; Siefer, G.; Wekkeli, A.; Welser, E.; Oliva, E.; Bett, A.; Dimroth, F. *Appl. Phys. Lett.* **2009**, *94*, 223504.
(5) Kingston, R. *Phys. Rev.* **1955**, *98*, 1766–1775.
(6) Montgomery, H.; Brown, W. *Phys. Rev.* **1956**, *103*, 865–870.
(7) Bohr, M.; Chao, R.; Ghani, T.; Mistry, K. *IEEE Spectrum* **2007**, *44*, 29.
(8) Cullen, G.; Amick, J.; Gerlich, D. *J. Electrochem. Soc.* **1962**, *109*, 124–127.
(9) Rivillion, S.; Chabal, Y. J.; Amy, F.; Kahn, A. *Appl. Phys. Lett.* **2005**, *87*, 253101.
(10) Loscutoff, P. W.; Bent, S. F. *Annu. Rev. Phys. Chem.* **2006**, *57*, 467–495.
(11) Anderson, G.; Hanf, M.; Norton, P.; Lu, Z.; Graham, M. *Appl. Phys. Lett.* **1995**, *66*, 1123–1125.
(12) Houssa, M.; Nelis, D.; Hellin, D.; Pourtois, G.; Conard, T.; Paredis, K.; Vanormelingen, K.; Vantomme, A.; Van Bael, M.; Mullens, J.; Caymax, M.; Meuris, M.; Heyns, M. *Appl. Phys. Lett.* **2007**, *90*, 222105.
(13) Hanrath, T.; Korgel, B. *J. Am. Chem. Soc.* **2004**, *126*, 15466–15472.
(14) Newstead, K.; Robinson, A.; Patchett, A.; Prince, N.; McGrath, R.; Whittle, R.; Dudzik, E.; McGovern, J. T. *J. Phys: Condens. Matter* **1992**, *4*, 8441–8446.
(15) Lyman, P.; Sakata, O.; Marasco, D.; Breneman, K.; Keane, D.; Bedzyk, M. *Surf. Sci.* **2000**, *462*, L594–L598.
(16) Ardalan, P.; Musgrave, C.; Bent, S. *Langmuir* **2009**, *25*, 2013–2025.
(17) Buriak, J. M. *Chem. Rev.* **2002**, *102*, 1271–1308.
(18) Kosuri, M.; Cone, Q. R.; Li, S. M. H.; Bunker, B.; Mayer, T. *Langmuir* **2004**, *20*, 835–840.
(19) Linford, M.; Fenter, P.; Eisenberger, P.; Chidsey, C. *J. Am. Chem. Soc.* **1995**, *117*, 3145–3155.
(20) Sharp, I.; Schoell, S.; Hoeb, M.; Brandt, M.; Stutzmann, M. *Appl. Phys. Lett.* **2008**, *92*, 223306.
(21) Choi, K.; Buriak, J. *Langmuir* **2000**, *16*, 7737–7741.
(22) Gorositza, P.; Henry de Villeneuve, C.; Sun, Q.; Sanz, F.; Wallart, X.; Boukherroub, R.; Allongue, P. *J. Phys. Chem. B* **2006**, *110*, 5576–5585.
(23) Bansal, A.; Li, X.; Lauermann, I.; Lewis, N.; Yi, S.; Weinberg, W. *J. Am. Chem. Soc.* **1996**, *118*, 7225–7226.
(24) Bansal, A.; Lewis, N. *J. Phys. Chem. B* **1998**, *102*, 4058–4060.
(25) Royea, W. J.; Juang, A.; Lewis, N. S. *Appl. Phys. Lett.* **2000**, *77*, 1988–1990.
(26) Yu, H.; Webb, L.; Heath, J.; Lewis, N. *Appl. Phys. Lett.* **2006**, *88*, 252111.
(27) Webb, L.; Lewis, N. *J. Phys. Chem. B* **2003**, *107*, 5404–5412.
(28) Seitz, O.; Boecking, T.; Salomon, A.; Gooding, J.; Cahen, D. *Langmuir* **2006**, *22*, 6915–6922.
(29) Salomon, A.; Boecking, T.; Seitz, O.; Markus, T.; Amy, F.; Chan, C.; Zhao, W.; Cahen, D.; Kahn, A. *Adv. Mater.* **2007**, *19*, 445–450.
(30) Scheres, L.; Giesbers, M.; Zuilhof, H. *Langmuir* **2009**, *26*, 4790–4795.
(31) Feng, W.; Miller, B. *Langmuir* **1999**, *15*, 3152–3156.
(32) Faucheux, A.; Yang, F.; Allongue, P.; Henry de Villeneuve, C.; Ozanam, F.; Chazalviel, J.-N. *Appl. Phys. Lett.* **2006**, *88*, 193123.
(33) Moraillon, A.; Gouget-Laemmel, A.; Ozanam, F.; Chazalviel, J.-N. *J. Phys. Chem. C* **2008**, *112*, 7158–7167.
(34) Tobia, D.; Baranski, J.; Rickborn, B. *J. Org. Chem.* **1989**, *54*, 4253–4256.
(35) Haber, J. A.; Lewis, N. S. *J. Phys. Chem. B* **2002**, *106*, 3639–3656.
(36) Sze, S. *Physics of Semiconductor Devices*, 2nd ed.; John Wiley & Sons: New York, 1981.
(37) Many, A.; Goldstein, Y.; Grover, N. *Semiconductor Surfaces*; North-Holland Publishing Co.: Amsterdam, 1965.
(38) Yablonovitch, E.; Allara, D.; Chang, C.; Gmitter, T.; Bright, T. *Phys. Rev. Lett.* **1986**, *57*, 249–252.
(39) Nemanick, E.; Hurley, P.; Brunschwig, B.; Lewis, N. *J. Phys. Chem. B* **2006**, *110*, 14800–14808.
(40) Shewchun, J.; Dubow, J.; Myszkowski, A.; Singh, R. *J. Appl. Phys.* **1978**, *49*, 855–864.
(41) Hunger, R.; Fritsche, R.; Jaeckel, B.; Jaegermann, W.; Webb, L.; Lewis, N. *Phys. Rev. B* **2005**, *72*, 045317.
(42) Chen, R.; Bent, S. *Chem. Mater.* **2006**, *18*, 3733.
(43) Rivillion, S.; Chabal, Y. *J. Phys. IV* **2006**, *132*, 195–198.
(44) Lu, Z. *Appl. Phys. Lett.* **1996**, *68*, 1996.
(45) He, J.; Lu, Z.; Mitchell, S.; Wayner, D. *J. Am. Chem. Soc.* **1998**, *120*, 2660–2661.
(46) Fellah, S.; Boukherroub, R.; Ozanam, F.; Chazalviel, J.-N. *Langmuir* **2004**, *20*, 6359–6364.
(47) Bailey, W.; Patricia, J. *J. Organomet. Chem.* **1988**, *352*, 1–46.
(48) Gerlich, D.; Cullen, G.; Amick, J. *J. Electrochem. Soc.* **1962**, *109*, 133–138.
(49) Wang, S.; Wallis, G. *Phys. Rev.* **1957**, *107*, 947–953.
(50) Tsipas, P.; Dimoulas, A. *Appl. Phys. Lett.* **2009**, *94*, 012114.
(51) Broqvist, P.; Alkauska, A.; Pasquarello, A. *Phys. Rev. B* **2008**, *78*, 075203.
(52) Houssa, M.; Chagarov, E.; Kummel, A. *MRS Bull.* **2009**, *34*, 504.
(53) Lopinski, G.; Eves, B.; Hul'ko, O.; Mark, C.; Patitsas, N.; Boukherroub, R.; Ward, T. *Phys. Rev. B* **2005**, *71*, 125308.
(54) Cao, P.; Yu, H.; Heath, J. *J. Phys. Chem. B* **2006**, *110*, 2006.
(55) Webb, L.; Rivillon, S.; Michalak, D.; Chabal, Y.; Lewis, N. *J. Phys. Chem. B* **2006**, *110*, 7349–7356.
(56) Jaeckel, B.; Hunger, R.; Webb, L.; Jaegermann, W.; Lewis, N. *J. Phys. Chem. C* **2007**, *111*, 18204–18213.
(57) Maldonado, S.; Plass, K.; Knapp, D.; Lewis, N. *J. Phys. Chem. C* **2007**, *111*, 17690–17699.

JP101375X